



Contents lists available at ScienceDirect

# Ultrasonics

journal homepage: [www.elsevier.com/locate/ultras](http://www.elsevier.com/locate/ultras)



## Multi-modal particle manipulator to enhance bead-based bioassays

P. Glynne-Jones<sup>a</sup>, R.J. Boltryk<sup>a,\*</sup>, M. Hill<sup>a</sup>, F. Zhang<sup>b</sup>, L. Dong<sup>b</sup>, J.S. Wilkinson<sup>b</sup>, T. Brown<sup>c</sup>,  
T. Melvin<sup>b</sup>, N.R. Harris<sup>d</sup>

<sup>a</sup>School of Engineering Sciences, University of Southampton, Southampton SO17 1BJ, UK

<sup>b</sup>Optoelectronics Research Centre, University of Southampton, Southampton SO17 1BJ, UK

<sup>c</sup>School of Chemistry, University of Southampton, Southampton SO17 1BJ, UK

<sup>d</sup>School of Electronics and Computer Science, University of Southampton, Southampton SO17 1BJ, UK

### ARTICLE INFO

*Article history:*  
Received 3 July 2009  
Received in revised form 23 September 2009  
Accepted 23 September 2009  
Available online xxxx

*PACS:*  
43.90.v

*Keywords:*  
Acoustic radiation forces  
Bio-sensor  
Frequency switching  
Micro-beads  
Optical waveguide

### ABSTRACT

By sequentially pushing micro-beads towards and away from a sensing surface, we show that ultrasonic radiation forces can be used to enhance the interaction between a functionalised glass surface and polystyrene micro-beads, and identify those that bind to the surface by illuminating bound beads using an evanescent field generated by guided light.

The movement towards and immobilisation of streptavidin coated beads onto a biotin functionalised waveguide surface is achieved by using a quarter-wavelength mode pushing beads onto the surface, while the removal of non-specifically bound beads uses a second quarter-wavelength mode which exhibits a kinetic energy maximum at the boundary between the carrier layer and fluid, drawing beads towards this surface. This has been achieved using a multi-modal acoustic device which exhibits both of these quarter-wavelength resonances. Both 1-D acoustic modelling and finite element analysis has been used to design this device and to investigate the spatial uniformity of the field.

We demonstrate experimentally that 90% of specifically bound beads remain attached after applying ultrasound, with 80% of non-specifically bound control beads being successfully removed acoustically. This approach overcomes problems associated with lengthy sedimentation processes used for bead-based bioassays and surface (electrostatic) forces, which delay or prevent immobilisation. We explain the potential of this technique in the development of DNA and protein assays in terms of detection speed and multiplexing.

© 2009 Elsevier B.V. All rights reserved.

## 1. Introduction

Bead-based assays are becoming increasingly important in microfluidic sensor systems with the advantage that the bead surface forms a disposable sensing element and a high bead surface area coupled with active mixing. These assays may be realised using magnetic beads held in devices using magnetic forces [1], however acoustic radiation forces can be used to manipulate a wider range of beads, including magnetic and non-magnetic beads, as they rely on acoustic properties only. The approach also allows finer control over bead position. Despite the advantages that acoustically enhanced bioassays could bring, it remains a challenge to move beads consistently to the detection area and in a uniform pattern. Thus a thorough understanding of the 2-D nature of the acoustic field in such a system is needed to ensure that beads can be suitably controlled. In this paper we investigate the axial acoustic field distribution using a 1-D acoustic impedance transfer

model [2], and also finite element analysis to model the lateral variation of the field. Thus the uniformity and suitability of the 2-D field may be judged. To aid this assessment a simulation of force potential,  $\langle\phi(r)\rangle$ , is used to provide a means of predicting bead migration.

## 2. Device design

### 2.1. General

In order to enhance bead-based assays, it is proposed that acoustic radiation forces are used to (a) push beads to the detection surface and (b) discriminate between beads that bind to the surface and those that do not by subsequently repelling unbound beads. Fig. 1 illustrates two acoustic modes which provide these two functions. Firstly, Fig. 1a shows a “to reflector” quarter-wave mode, used to move beads to the detection surface and secondly Fig. 1b shows a “to carrier” quarter-wave mode, used to force beads off the surface. In both cases, there must be sufficient radiation force at the wall to enhance binding and to overcome surface

\* Corresponding author. Tel.: +44 (0) 238059 2896; fax: +44 (0) 238059 7322.  
E-mail address: [R.J.Boltryk@soton.ac.uk](mailto:R.J.Boltryk@soton.ac.uk) (R.J. Boltryk).

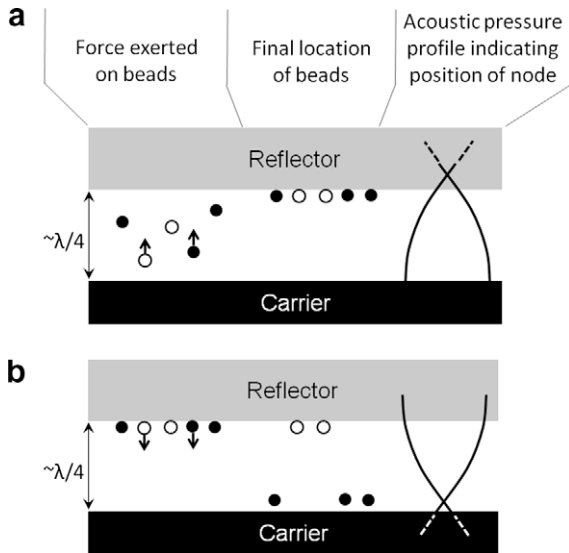


**Fig. 1.** Multi-modal function of device showing force on beads, final location and pressure field for (a) “to reflector” mode; beads and immobilised bio-molecules move up to waveguide surface whereupon functionalised beads (○) will attach to the reflector surface, and (b) “to carrier” mode; unbound beads (●) are pulled away and towards the carrier layer surface.

forces, which dictates where pressure nodes and antinodes are positioned in relation to the surface (noting that radiation force is typically zero at these nodal points). Fig. 1 therefore also indicates how the “to carrier” nodal points have been positioned some way into the reflector surface to ensure that beads are forced onto the surface.

### 2.2. Transfer impedance 1-D model

The final design was arrived at through successive iterations, investigating the behaviour as predicted by a 1-D transfer impedance model [2] implemented in MATLAB. This represents the structure as a layered resonator with layers of infinite lateral extent, thus ignoring any lateral acoustic modes.

This is sufficiently accurate, however, to arrive at a suitable multi-modal design. The transducer representation used by Hill et al. [2] was replaced by a KLM circuit model [3] extending the operating frequency of the model beyond the first resonance. For each design iteration, the average acoustic energy density (see equations below) in the fluid layer versus frequency is inspected; this allows all the resonances supported by that configuration to be identified and examined to determine their resultant acoustic force potential. Of the modes described in Fig. 1, the reflector quarter-wave mode is found to be the most sensitive to geometry, so it was easier to start the process with a design that easily supported this mode, with subsequent changes aiming to enhance the strength of the carrier layer quarter-wave mode.

These design iterations produced the final design depicted in Fig. 2, whose layer thicknesses are recorded in Table 1. The chamber floor is formed from macor, a machinable ceramic, with a PZT transducer (a 10 mm diameter disc of PZT26, Ferroperm) glued (Epotek 301 epoxy) to the reverse side. The walls of the fluidic chamber (chamber 5 mm in diameter) are formed by a moulded PDMS gasket to prevent the steel spacer coming into fluidic contact with the sample, and also to reduce the strength of lateral acoustic modes that cause variations in the radiation force across the width of the device. The roof of the chamber (the acoustic reflector) is formed by a sheet of BK7 glass. Fluidic connections are supplied via a PMMA manifold which connects to the fluidic chamber via

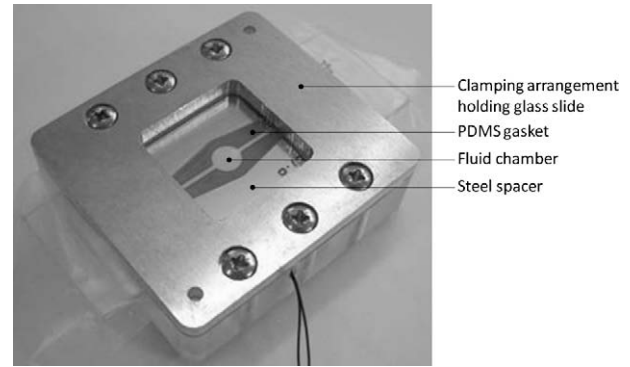


**Fig. 2.** Photograph of particle manipulator device showing the main fluid chamber capped by a glass slide.

**Table 1**  
Geometry of device.

Layer	Material	Thickness (μm)	Density (kg/m <sup>3</sup> )	Sonic velocity (m/s)
Transducer	PZ26	1000	7700	4529
Carrier	Alumina	650	3860	10,520
Fluid	Water	162	1000	1480
Reflector	BK7 glass <sup>a</sup>	1762 <sup>a</sup>	2500	5872

<sup>a</sup> Thickness and properties chosen for optical detection system.

ports in the macor layer, with PDMS gaskets to seal the connection. An aluminium clamp holds the assembly together. The ultrasonic transducer is powered by an RF-amplifier (ENI 240L) driven by a sine-wave from a signal generator (TTi TG1304).

Troughs in the resulting modelled impedance data are indicative of a resonance and clearly show two modes (Fig. 3), the peaks in the acoustic energy density in the fluid confirm that they are resonances directly associated or coupled with the fluid layer. These correspond to the carrier quarter-wave and reflector quarter-wave modes which are located at 1.57 and 1.70 MHz respectively. The smaller energy density associated with the reflector quarter-wave mode is indicative of the design challenge that this mode presents.

### 2.3. Finite element (FE) model

In order to gain a more detailed understanding of the behaviour of the device, including lateral forces, an axisymmetric finite element model was implemented using the ANSYS package.

#### 2.3.1. Construction of model

The modelling of lateral fields has been described by Neild et al. [4], Manneberg et al. [5], Lilliehorn et al. [6], Hagsater et al. [7] and Townsend et al. [8], and this work extends that of Townsend, incorporating a finite element representation of the transducer and using the results to visualise the force distribution in three-dimensions. Even in layered resonator designs which are most suited to a one-dimensional approach, significant lateral variations in acoustic radiation forces can be observed [8], which finite element analysis could be used to model.

A full verification of this finite element approach is beyond the scope of this paper, but Fig. 4 represents some initial verification: it compares the transfer impedance model to a finite element model with boundary conditions set to mimic layers of infinite extent. The finite element model is based in ANSYS [9], and uses a strip of FLUID29 (2-D harmonic acoustic) elements; carrier and reflector layers are represented by 2-D structural solid elements, PLANE42; and the PZT by the piezoelectric formulation of the 2-D Coupled-

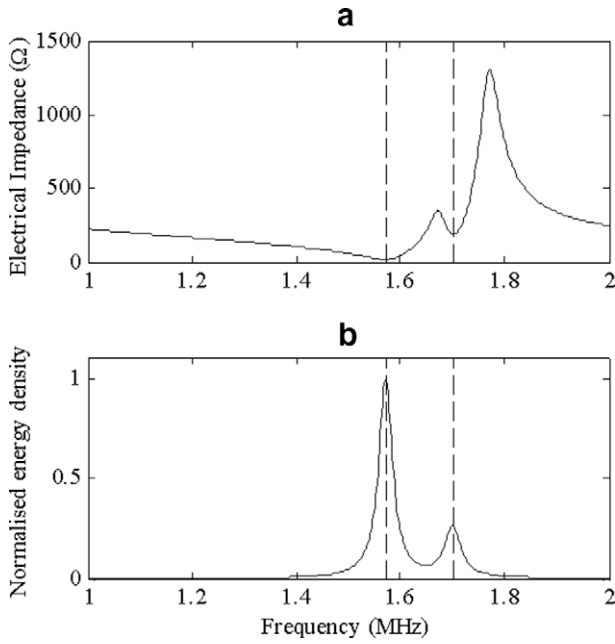


Fig. 3. MATLAB 1-D model results for (a) magnitude of electrical impedance and (b) acoustic energy density within the fluid layer. Dashed lines correspond to predicted resonant modes at 1.572 MHz and 1.700 MHz.

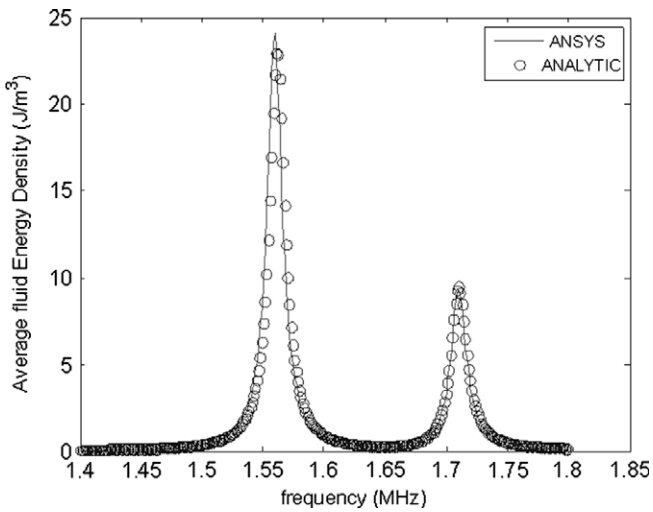


Fig. 4. Predicted acoustic energy density for 1-D system and comparison between FE and transfer impedance models.

Field Solid PLANE13. Varying the parameters of the transmission line model, it is found that for the parameters considered here, the air beyond the reflector and transducers has little effect on the energy density profile, and is not included in the ANSYS model. The acoustic fluid elements are not formulated to allow any fluid damping in the fluid body, which makes predictions of acoustic amplitudes less accurate, particularly for half-wave devices where the fluid damping is important, however in the future, other element types such as FLUID79 which can include fluid damping will be explored in the future. All materials data is taken from manufacturers' data tables. The figure contains two maxima in the time averaged fluid energy density corresponding to the 'to carrier' and 'to reflector' quarter-wave modes. It can be seen that there is good agreement between the two types of model.

For the axisymmetric model shown in Fig. 5, the same element types were used; the additional spacer layer was also represented

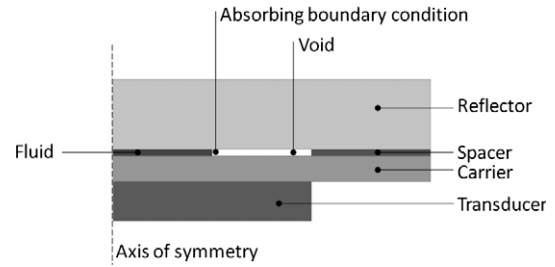


Fig. 5. Construction of FE model (ANSYS).

by PLANE42 elements. The dimensions of the model are as listed in Table 1, the radius of the modelled reflector and carrier layer was 80 mm and the transducer radius 25 mm; the spacer as an annulus of inner and outer radii 50 mm and 80 mm respectively. The region between the fluid and the spacer is physically composed of a PDMS gasket and some air spaces; in order to mimic the energy scattering nature of this region (to acoustic energy from the fluid), the right-side of the fluid layer is bounded by a 50% absorbing boundary condition with the remaining space left as a void in the model, as it is anticipated that the gasket and air will have little effect on the dynamics of the surrounding material.

### 2.3.2. Calculation of force potential

For a harmonically varying sound field, where the fluid particle velocity,  $u$ , has amplitude  $U$  and fluid pressure,  $p$ , has amplitude  $P$ , the time averaged kinetic and potential energy densities can be calculated [10] as

$$\langle \bar{E}_{kin}(r) \rangle = \frac{1}{4} \rho_0 U^2, \quad (1)$$

and

$$\langle \bar{E}_{pot}(r) \rangle = \frac{1}{4} \frac{P^2}{\rho_0 c^2}, \quad (2)$$

where  $\rho_0$  is the density of the fluid, and  $c$  the speed of sound in the fluid.

Post-processing of the FLUID29  $u$  and  $p$  output parameters allows these equations to be implemented. The following equations derived by Gor'kov [11] allow the radiation force to be derived from an arbitrary standing wave field and the acoustic potential and energy densities. The acoustic radiation force (a time averaged quantity) is given by [12]

$$\langle F(r) \rangle = -\nabla \langle \phi(r) \rangle, \quad (3)$$

where the force potential,  $\langle \phi(r) \rangle$ , is given by

$$\langle \phi(r) \rangle = -V \left[ \frac{3(\lambda - 1)}{2\lambda + 1} \langle \bar{E}_{kin}(r) \rangle - \left( 1 - \frac{1}{\sigma^2 \lambda} \right) \langle \bar{E}_{pot}(r) \rangle \right], \quad (4)$$

and where  $\lambda$  is the ratio of particle density to fluid density,  $\sigma$  the ratio of speed of sound in the particle to that in the fluid and  $V$  the particle volume.

### 2.3.3. Simulation results

Plotting the acoustic force potential,  $\langle \phi(r) \rangle$ , is a convenient way of visualising the acoustic forces. A particle will tend to move towards regions where  $\langle \phi(r) \rangle$  is low (indicated black in Fig. 6) with a force proportional to the spacings of plotted contour lines.

Fig. 6 shows the force potential in the fluid for three modes, where the left boundary represents the centre of the chamber and right boundary the gasket wall (fluid elements shown in Fig. 5). The frequencies at which these modes appear are listed in Table 2 where they are compared with the 1-D model and experimental results. Fig. 6a and b are both "to carrier" quarter-wave

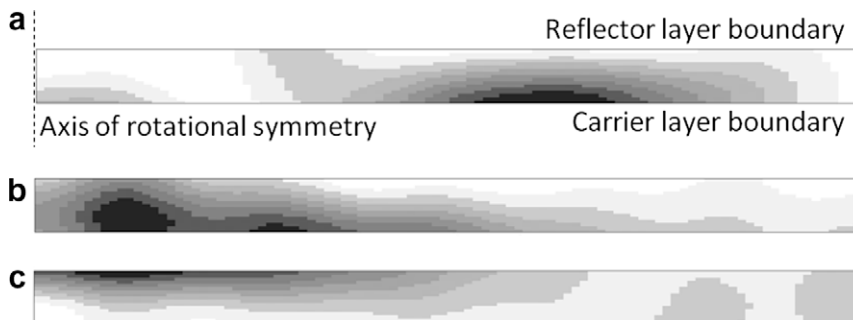


Fig. 6. Plots of force potential in fluid layer elements (see Fig. 4) where black indicates agglomeration region for (a) 1.55 MHz “to carrier” quarter-wave, (b) 1.61 MHz “to carrier” quarter-wave and (c) 1.72 MHz “to reflector” quarter-wave.

218 modes, and show strong variation across the width of the device.  
219 Fig. 6c shows a “to reflector” quarter-wave, and predicts that the  
220 forces will be stronger nearer the centre of the chamber. This is ob-  
221 served in practice, although the pattern of force variation is more  
222 complex than the model predicts. This is probably due to poorly  
223 matched boundary conditions – both of the energy dissipation of  
224 the gasket, and the complex nature of the clamping that is not re-  
225 flected in the model. The main uses of the model are to provide  
226 indications of the type of variation to be expected, and give in-  
227 sights into the causes of these variations. In particular we note that  
228 surface and plate-wave type mode shapes have a strong influence  
229 on lateral behaviour. In the future we will use the finite element  
230 models to develop designs that are less sensitive to geometric vari-  
231 ations and material parameters to produce manipulation devices  
232 that produce more uniform action over a chamber area.

### 233 3. Enhancement of microbead assay

234 This section describes how the multimodal operation can be  
235 used to assist microbead based assays. In this example, a mixture  
236 of 6 μm diameter streptavidin functionalised polystyrene beads  
237 (Bangs labs, CP01N) and non-functionalised fluorescent control  
238 beads (Invitrogen, P24671, 6 μm diameter, Cy5.5 labelled) are dri-  
239 ven against a glass reflector which has been functionalised with a  
240 PEG–biotin coating. The “to carrier” quarter-wave is then applied  
241 to remove the unbound control beads. In a more realistic applica-  
242 tion, the beads could be replaced by bacteria, and an antibody  
243 functionalised surface used. The finite element modelling predicts  
244 weakening axial forces at the chamber edges and the existence of  
245 complex lateral variations, particularly for the “to carrier” mode.  
246 These variations may also be aggravated by inlet channel geometry  
247 which results in asymmetric boundary conditions. However an  
248 area of approximately 1 mm<sup>2</sup> was found near the centre of the  
249 chamber where both the required acoustic modes were reasonably  
250 uniform. White light was coupled into the glass reflector through  
251 its end face such that an evanescent field was established close  
252 to the surface. This evanescent field illuminates any beads in direct  
253 contact with the reflector. An epifluorescent microscope was used  
254 to distinguish between the streptavidin beads and the fluorescent  
255 control beads.

256 The biotin surface functionalisation was performed as follows:  
257 initially the glass slide surface was cleaned by sequentially  
258 immersing it with ultrasonic agitation in ethanol, isopropanol, then  
259 de-ionized water, 10 min at each step, with further rinsing in de-  
260 ionized water. The surface was activated by immersing the slide  
261 in a piranha etch for 15 min. Silanization was performed by  
262 immersing the slide for 3 h in a 0.1% solution of 3-aminopropyl-tri-  
263 methoxysilane at room temperature. Finally, the slide was soaked  
264 for 3 h in a 0.2% solution of biotin–PEG–NHS, Mr 3400 (Creative  
265 PEGWorks, USA).

Table 2  
Frequencies of operation (MHz).

Mode	1-D model (MATLAB)	FE model (ANSYS)	Measured
“To carrier”	1.572	1.55 and 1.61	1.508
“To reflector”	1.700	1.72	1.712

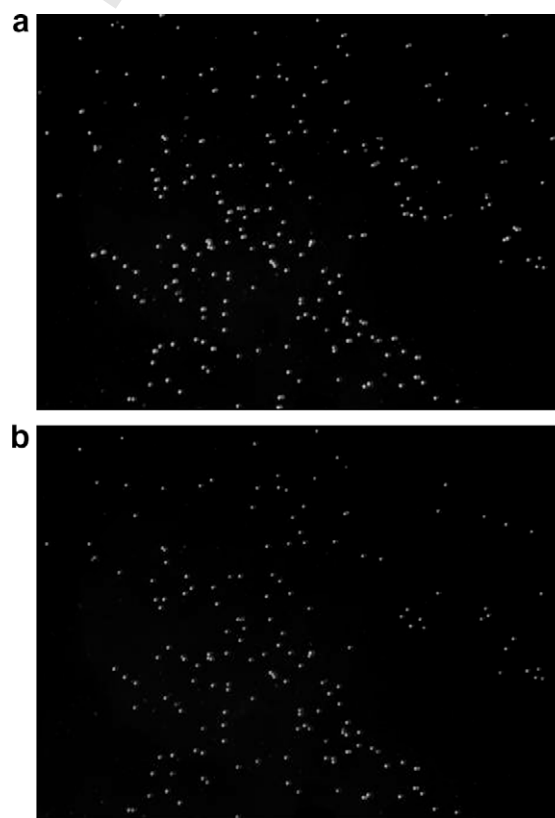


Fig. 7. Microscope images of control and streptavidin coated beads located on reflector surface after (a) initial application of “to reflector” quarter-wave and (b) subsequent application of “to carrier” quarter-wave excitation.

266 Drive voltages were set to 19 Vpp. The strength of the radiation  
267 forces were measured using the force balance method described by  
268 Martin et al. [13] whereby drive voltage is reduced until the radi-  
269 ation force is just balanced by the sedimentation force. At  
270 19 Vpp, this predicts forces of approximately 4.1 and 10.1 pN for  
271 the to reflector and to carrier modes respectively. These values  
272 have an estimated error of 8%, associated with the difficulty in

distinguishing between a particle sedimenting very slowly and one still being held.

After applying the “to reflector” quarter-wave, all beads were seen to reach the surface within 1 s of activation (Fig. 7a). After a 90 s delay to ensure bead capture, excitation was switched to the “to carrier” mode (Fig. 7b). Based on the images collected over a series of five repeated experiments, it was found that this removed 80% ( $\pm 9\%$ ) of the control beads, while 90% ( $\pm 6\%$ ) of the streptavidin beads remained attached to the surface. A short 0.5 s burst of 2 mm s<sup>-1</sup> flow through the chamber was sufficient to dislodge further Cy5.5 labelled control beads, such that 92% of them in total were removed. This compares to the case when no ultrasound was used, where even after 270 s only a small proportion of the beads were seen to be in contact with the waveguide surface, the remainder possibly repelled by electrostatic forces. These results show that this technique could provide a new and useful type of rapid assay. It should be noted that no efforts were made to optimise the surfaces and experimental conditions to reduce non-specific binding to a level that would be necessary for practical assays – rather these experiments seek to show proof of concept.

#### 4. Conclusion

In the device presented, both quarter-wavelength modes have been demonstrated and at frequencies which tally closely with modelled results. These modes have been shown to significantly enhance the immobilisation of functionalised beads, with all beads brought to the surface within 1 s.

A 3-D finite element model incorporating both the piezoelectric and acoustic interactions has been verified against a layered device. Applying this to an axisymmetric model of the manipulator device we obtain useful insights into the action of the device. It predicts the type of lateral force variations that are observed experimentally, but further work to improve the way boundary conditions and damping are modelled is required before we can be confident in the modelled results. The model is sufficiently accurate to be useful in the future for developing designs that

are less sensitive to geometric variations and material parameters, and to produce manipulation devices that produce more uniform action over a chamber area.

#### Acknowledgements

This work was supported by the EPSRC (Grant EP/D03454X/1), DSTL, Point Source, and Genetix Ltd.

#### References

- [1] N. Jaffrezic-Renault, C. Martelet, Y. Chevolut, J.P. Cloarec, Biosensors and bio-bar code assays based on biofunctionalized magnetic microbeads, *Sensors* 7 (2007) 589–614.
- [2] M. Hill, Y. Shen, J.J. Hawkes, Modelling of layered resonators for ultrasonic separation, *Ultrasonics* 40 (2002) 385–392.
- [3] R. Krimholt, D.A. Leedom, G.L. Matthaei, New equivalent circuits for elementary piezoelectric transducers, *Electronics Letters* 6 (1970) 398.
- [4] A. Neild, S. Oberti, A. Haake, J. Dual, Finite element modeling of a microparticle manipulator, *Ultrasonics* 44 (2006) e455–e460.
- [5] O. Manneberg, B. Vanherberghen, J. Svennebring, H.M. Hertz, B. Onfelt, M. Wiklund, A three-dimensional ultrasonic cage for characterization of individual cells, *Applied Physics Letters* 93 (2008) 063901.
- [6] T. Lilliehorn, U. Simu, M. Nilsson, M. Almqvist, T. Stepinski, T. Laurell, J. Nilsson, S. Johansson, Trapping of microparticles in the near field of an ultrasonic transducer, *Ultrasonics* 43 (2005) 293–303.
- [7] S.M. Hagsater, C.H. Westergaard, H. Bruus, J.P. Kutter, A compact viewing configuration for stereoscopic micro-PIV utilizing mm-sized mirrors, *Experiments in Fluids* 45 (2008) 1015–1021.
- [8] R.J. Townsend, M. Hill, N.R. Harris, N.M. White, Investigation of two-dimensional acoustic resonant modes in a particle separator, *Ultrasonics* 44 (2006) e467–e471.
- [9] ANSYS Inc., ANSYS™ Theory Reference Manual, Release 9.0, PA, USA, November 2004.
- [10] L.E. Kinsler, A.E. Frey, A.B. Coppens, J.V. Saunders, *Fundamentals of Acoustics*, third ed., Wiley, New York, 1982.
- [11] L.P. Gor'kov, On the forces acting on a small particle in an acoustical field in an ideal fluid, *Soviet Physics Doklady* 6 (1962) 773–775.
- [12] M. Gröschl, Ultrasonic separation of suspended particles – Part I: fundamentals, *Acustica* 84 (1998) 432–447.
- [13] S.P. Martin, R.J. Townsend, L.A. Kuznetsova, K.A.J. Borthwick, M. Hill, M.B. McDonnell, W.T. Coakley, Spore and micro-particle capture on an immunosensor surface in an ultrasound standing wave system, *Biosensors & Bioelectronics* 21 (2005) 758–767.